Supplement of Atmos. Chem. Phys., 22, 13137–13152, 2022
https://doi.org/10.5194/acp-22-13137-2022-supplement

Supplement of

Seasonal variation in nitryl chloride and its relation to gas-phase precursors during the JULIAC campaign in Germany

Zhaofeng Tan et al.

Correspondence to: Zhaofeng Tan (zh.tan@fz-juelich.de) and Roberto Sommariva (rs445@le.ac.uk)

Table S1. Median, interquartile range (25%-75% percentiles) and maximum concentrations of 15-min averaged $ClNO_2$, NO_2, O_3, aerosol surface area (S_a), and aerosol liquid water content (ALWC) concentrations during nighttime ($j_{NO3} < 1\times10^{-4}$ s^{-1}) in the different measurement periods of the JULIAC campaign.

		31 Jan – 8 Feb	4 – 31 Aug	9 – 30 Sep	1 – 25 Nov	1 – 31 Dec
$ClNO_2$ / pptv	Median	150	22	45	46	80
	25% – 75%	76 – 300	7 – 99	7 – 156	15 – 110	38 – 160
	Maximum	950	1410	1600	450	630
NO / ppbv	Median	0.13	0.20	0.35	0.18	N.A.
	25% – 75%	0.01 – 1.2	0.04 – 0.68	0.03 – 0.93	0.02 – 1.4	N.A.
	Maximum	33	6.4	12	19	N.A.
NO_2 / ppbv	Median	7.6	3.9	4.2	7.8	5.2
	25% – 75%	3.7 – 13	2.2 – 6.2	2.6 – 6.9	4.2 – 12.0	2.9 – 8.5
	Maximum	29	27	26	29	25
O_3 / ppbv	Median	25	36	27	16	25
	25% – 75%	17 – 32	27 – 48	22 – 33	9 – 24	15 – 31
	Maximum	38	100	64	36	42
T / °C	Median	4.4	20.8	16.7	8.0	8.4
	25% – 75%	2.1 –7.4	18 – 24	15 – 19	6 – 11	5 – 11
	Maximum	12	34	29	19	19
RH / %	Median	71	49	72	88	86
	25% – 75%	59 – 79	27 – 65	55 – 88	81 – 93	76 – 92
	Maximum	86	82	100	100	100
S_a /$\mu m^2/cm^3$	Median	49	68	54	43	N.A.
	25% – 75%	20 – 75	51 – 122	37 – 85	21 – 59	N.A.
	Maximum	144	323	345	108	N.A.
ALWC [a] / $\mu g/m^3$	Median	0.11	1.43	0.81	1.93	N.A.
	25% – 75%	0.10 – 0.14	0.85 – 2.28	0.63 – 1.37	0.98 – 5.86	N.A.
	Maximum	0.23	6.59	4.23	25.6	N.A.

[a] Aerosol liquid water content is calculated from ISORROPIA2 assuming the aerosol in metastable state using forward mode using as input the aerosol composition from AMS measurements (i.e. NH_4^+, SO_4^{2-}, NO_3^-, Cl^-), measured temperature and RH, as suggested by Song et al. (2018). Data with RH<40% are excluded in the calculation to justify the assumption of metastable state, which is the case for periods except August when 3% of the data has RH<40%.

Table S2. Mean aerosol composition measured by AMS during the intensive measurement periods of the JULIAC campaign.

Group		PM_1 µg/m^3	NO_3^- µg/m^3	SO_4^{2-} µg/m^3	NH_4^+ µg/m^3	Cl^- µg/m^3	Organic µg/m^3
Feb	Regional	0.97	0.24	0.10	0.09	0.01	0.53
	Long-Range	0.17	0.10	0.11	0.11	0.13	0.26
Aug	Regional	11.59	0.51	2.93	1.18	0.02	6.96
	Long-Range	3.83	0.20	1.03	0.41	0.01	2.17
Nov	Regional	4.63	1.09	0.76	0.50	0.05	2.23
	Long-Range	0.88	0.09	0.15	0.06	0.02	0.55

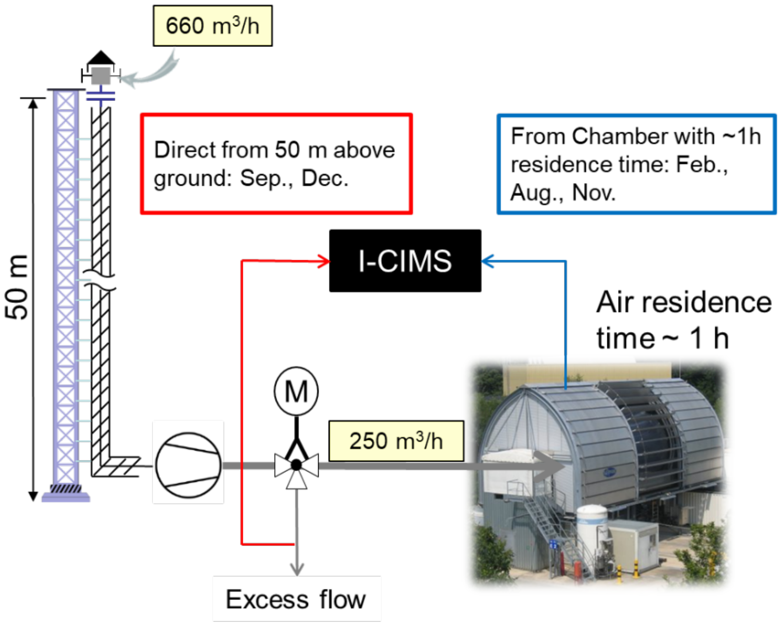

Figure S1. Schematic of the experimental setup of the JULIAC-SAPHIR system indicating the sampling points for the $ClNO_2$ measurements. During the intensive measurement periods of the JULIAC campaign (February, August, November), the I-CIMS instrument sampled from the SAPHIR chamber (blue line). Between the intensive measurement periods of the JULIAC campaign (September, December), the I-CIMS instrument sampled directly from the JULIAC tower (red line).

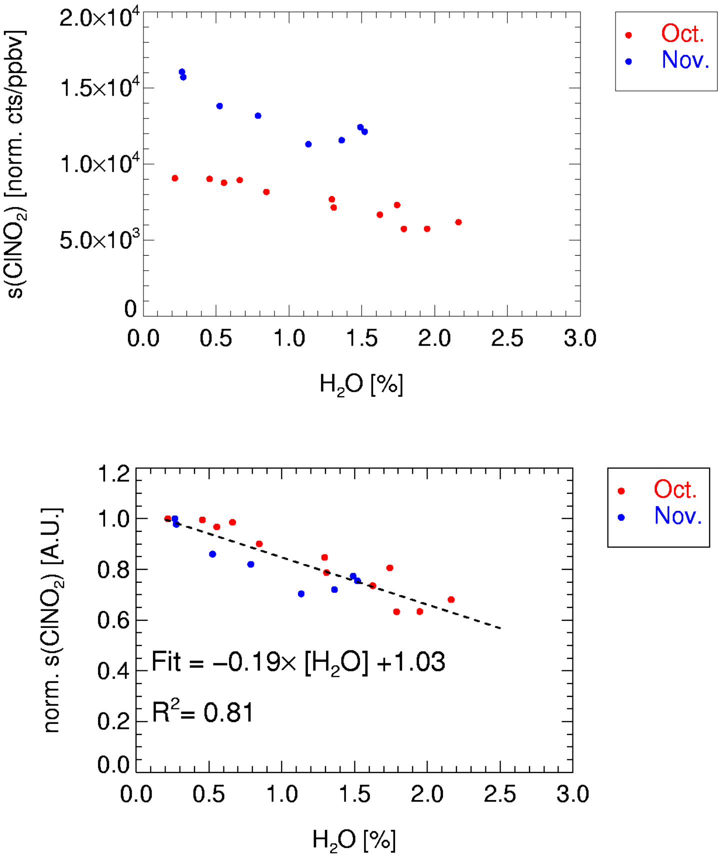

Figure S2. I-CIMS sensitivity dependence on the water vapor content determined in October and November during the JULIAC campaign. In calibration experiments, the inlet was overflowed with air containing a constant concentration of $ClNO_2$ (~5 ppbv) while varying the humidity. Upper panel: $ClNO_2$ signal (208 amu) normalized to the $(I{\cdot}(H_2O)^-)$ signal (145 amu) versus the H_2O mixing ratio by volume. Lower panel: Signals normalized to the maximum $ClNO_2$ signal $(s(ClNO_2)/s(ClNO_2)_{max})$. A linear fit is used to derive the humidity dependence giving a decrease in the instrument sensitivity of 19% per 1% H_2O concentration. The decreasing trend of the $ClNO_2$ signal with increasing humidity reflects the fact that the reaction of $ClNO_2$ with higher-order clusters of $I^-{\cdot}(H_2O)_n$ is slower than that with $I^-{\cdot}(H_2O)$ alone (Kercher et al., 2009;Slusher et al., 2004).

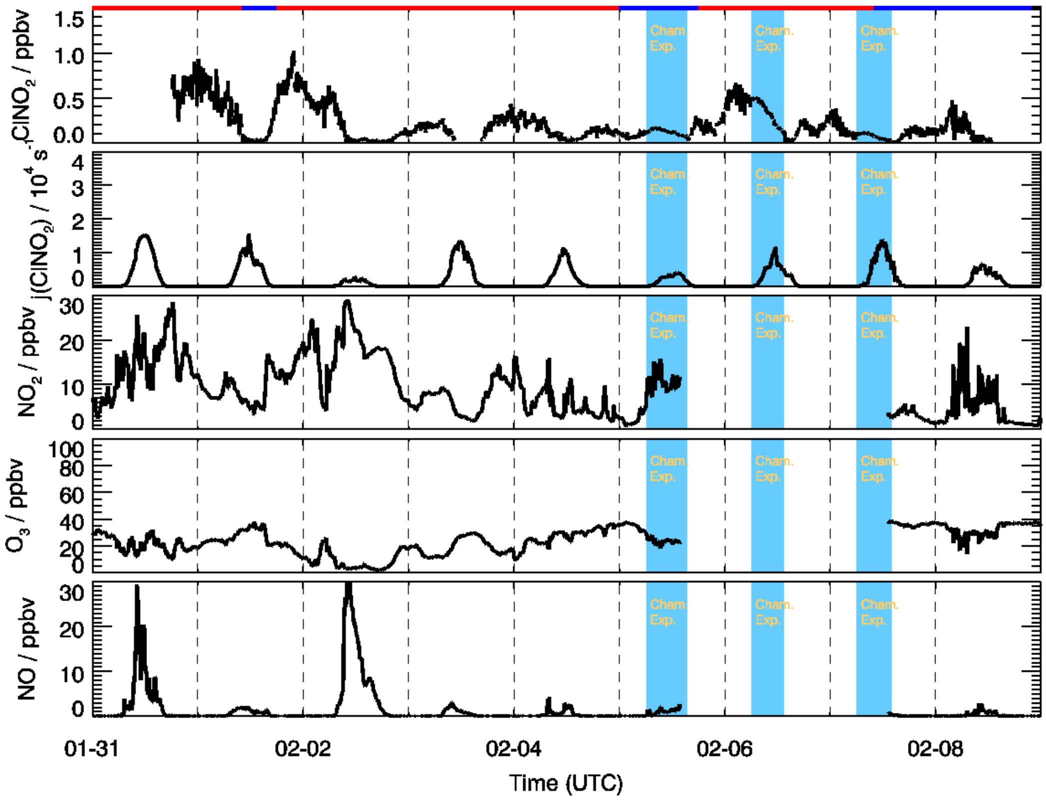

Figure S3. Time series of photolysis frequency j(ClNO$_2$), ClNO$_2$, NO$_2$, O$_3$, and NO concentrations in February of the JULIAC campaign. Horizontal blue and red lines indicate air mass from long-range (blue) and regional transportation (red), respectively (Section 3.2). The color filled areas indicate periods when characterization experiments were performed: these measurements were excluded from the analysis.

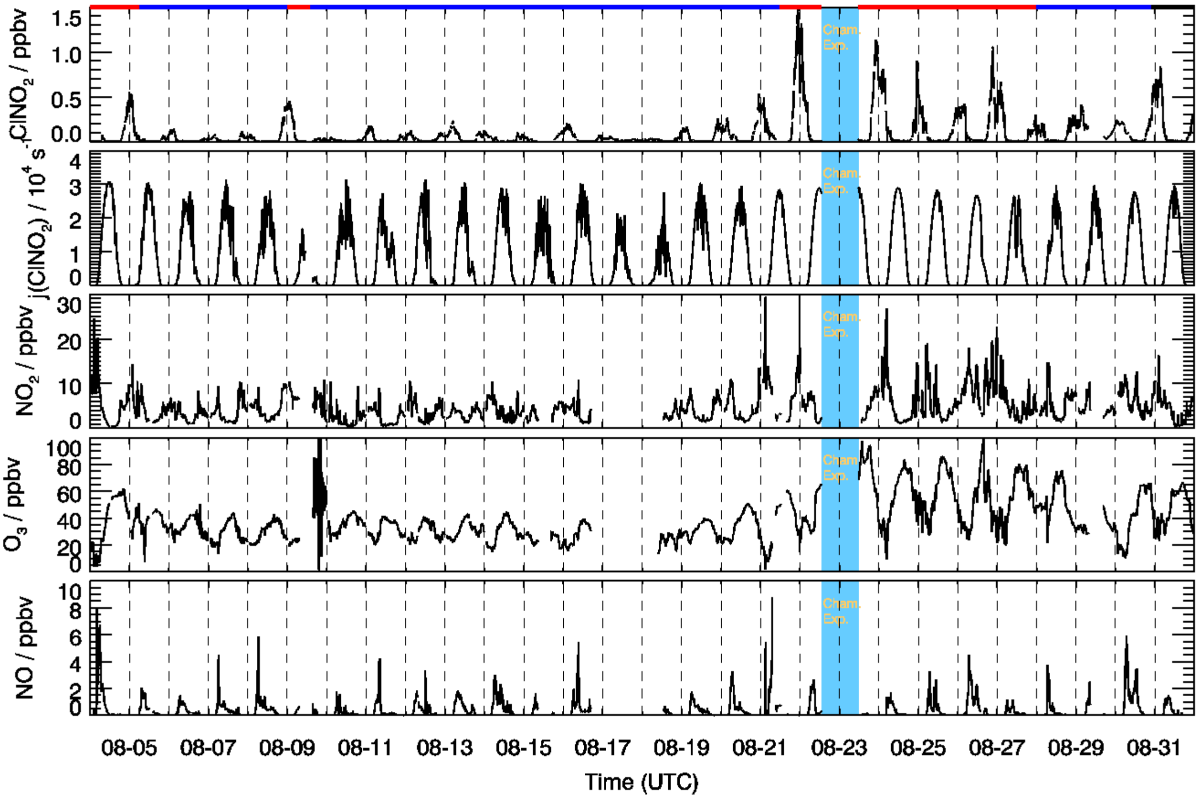

Figure S4. Same as Figure S3 but for the measurements in August.

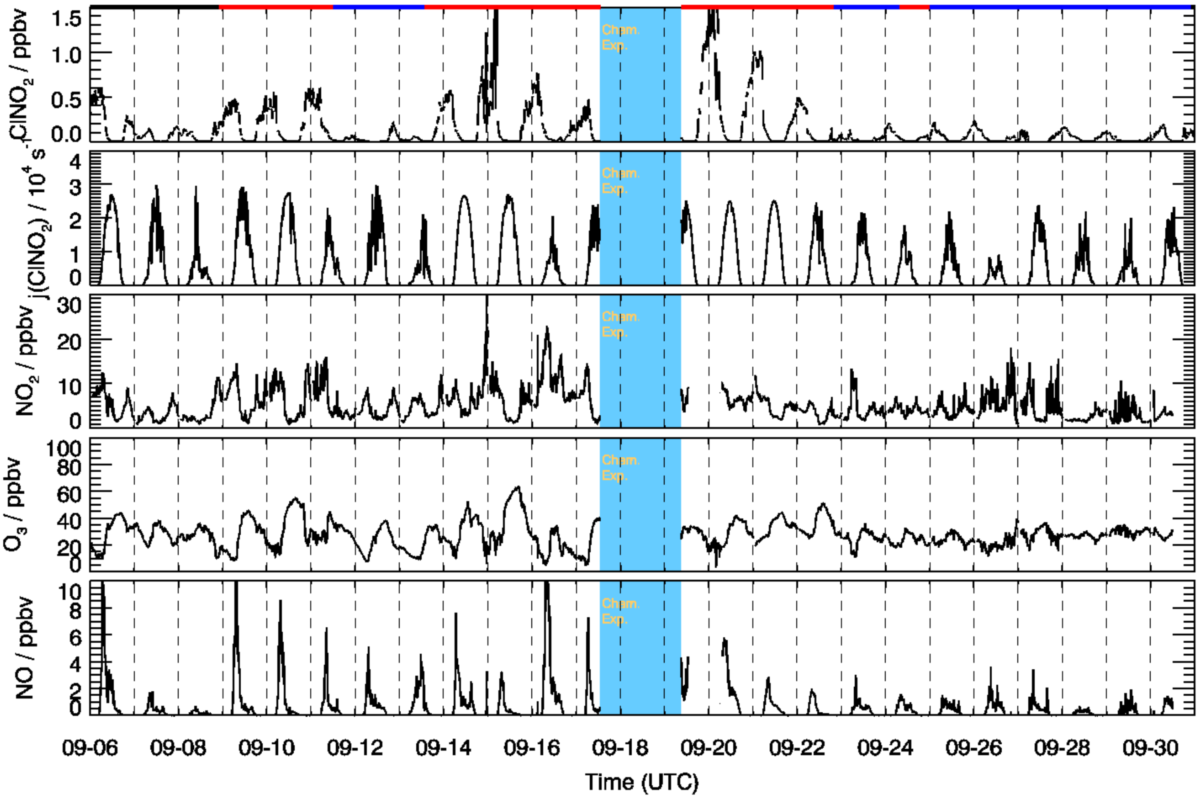

Figure S5. Same as Figure S3 but for the measurements in September.

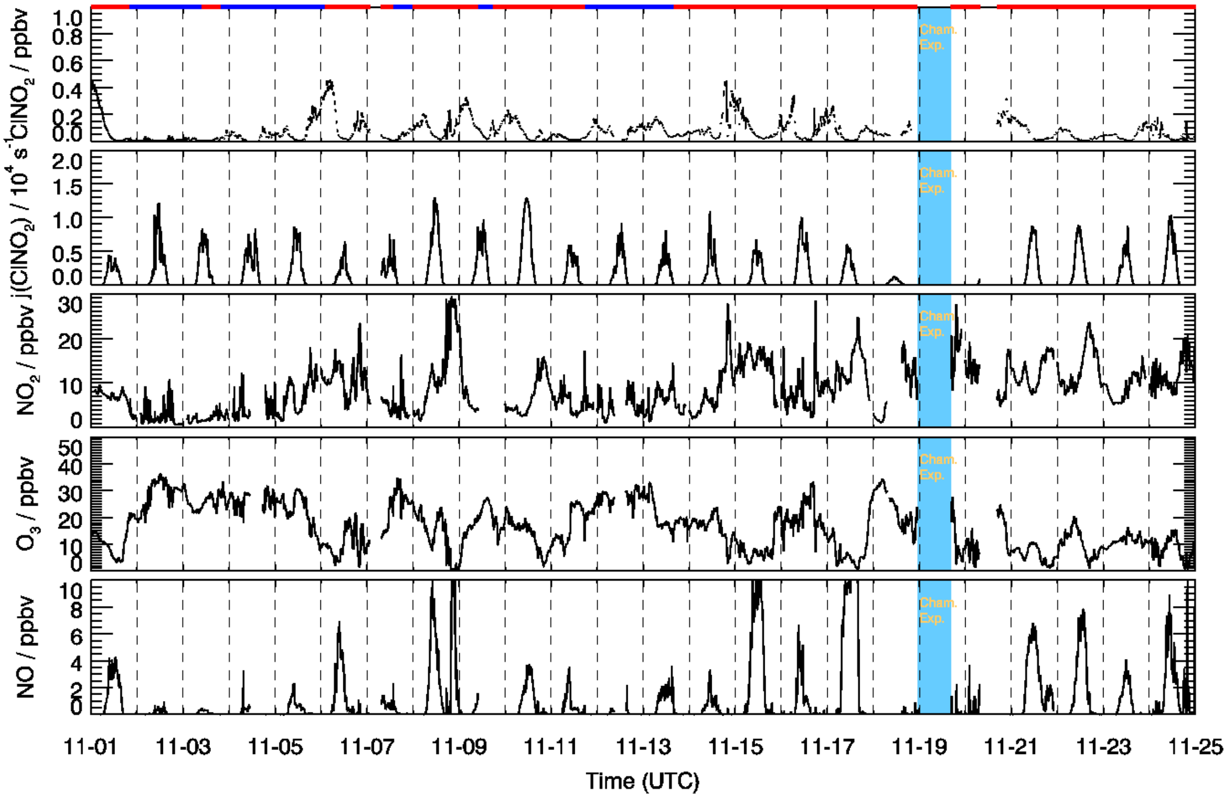

Figure S6. Same as Figure S3 but for the measurements in November.

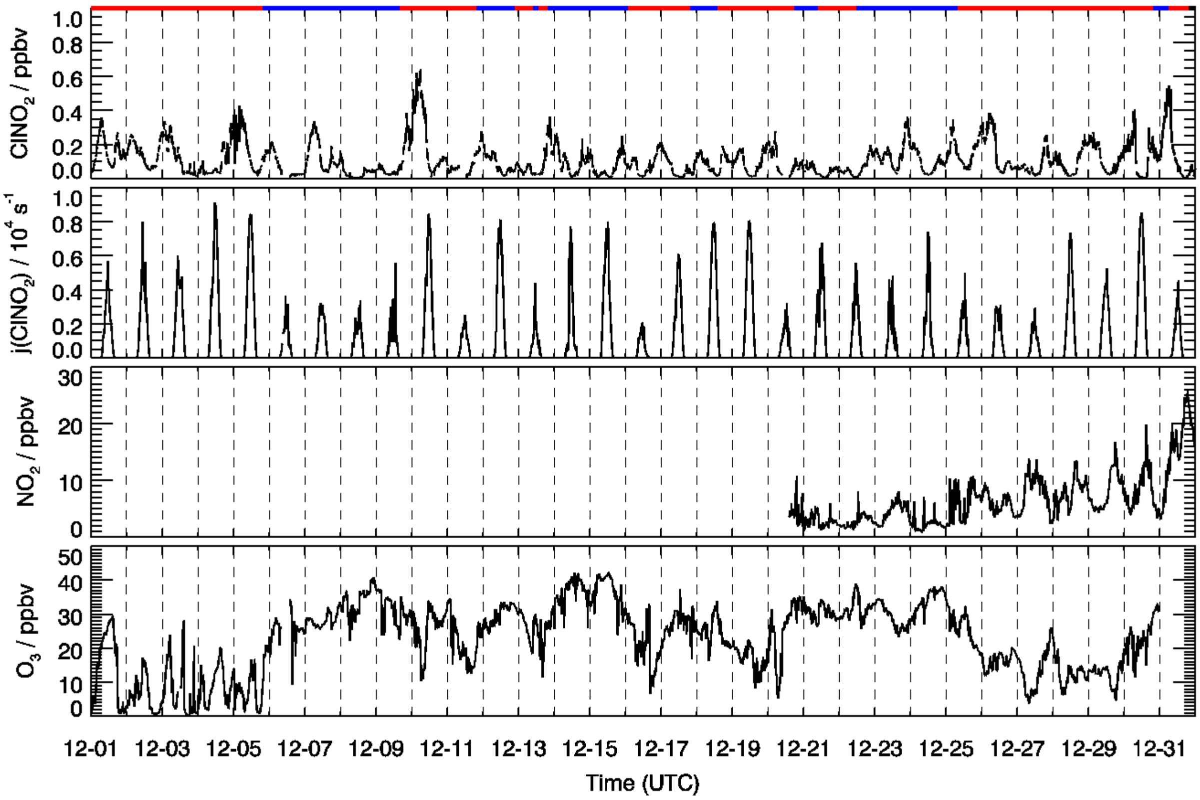

Figure S7. Same as Figure S3 but for the measurements in December. During this period NO measurements were not available.

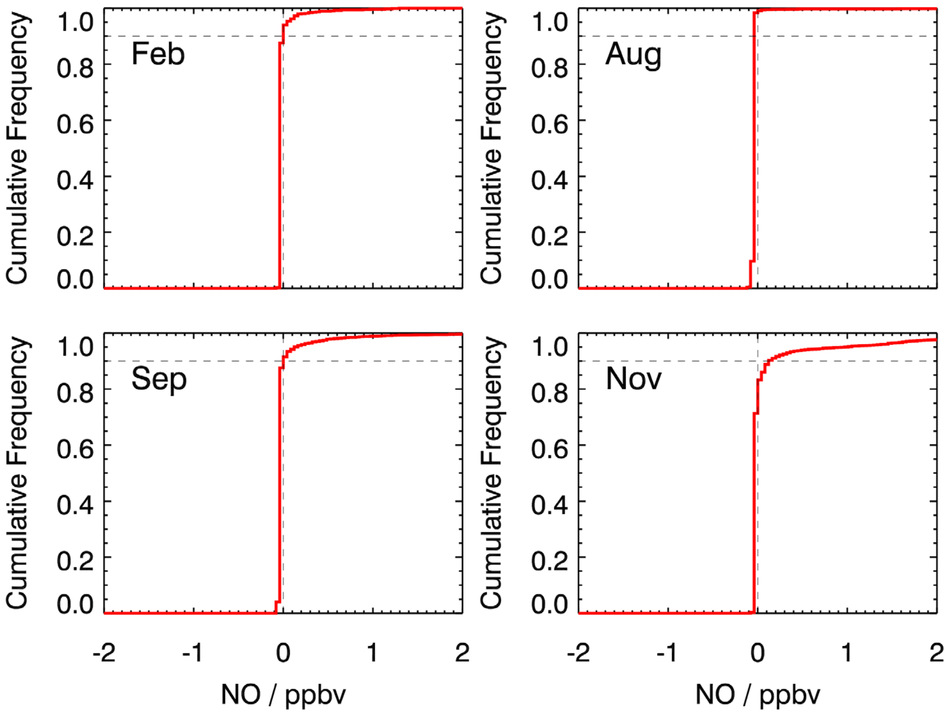

Figure S8. Cumulative histogram of measured NO concentrations during nighttime for different periods. The horizontal lines denote the position of 90% percentile of data.

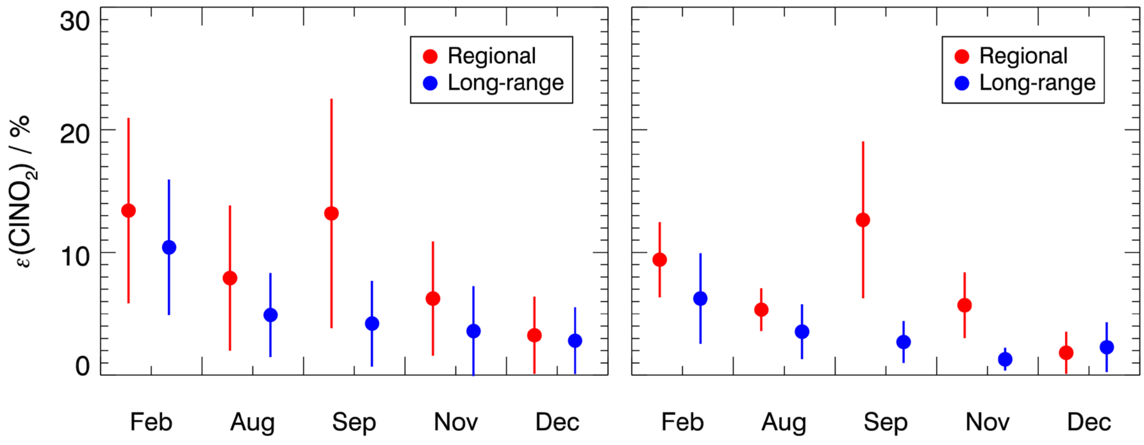

Figure S9. Same as Fig. 5 but for all nighttime data (left) and for data 1 hour (+/- 0.5h interval) before sunrise (right).

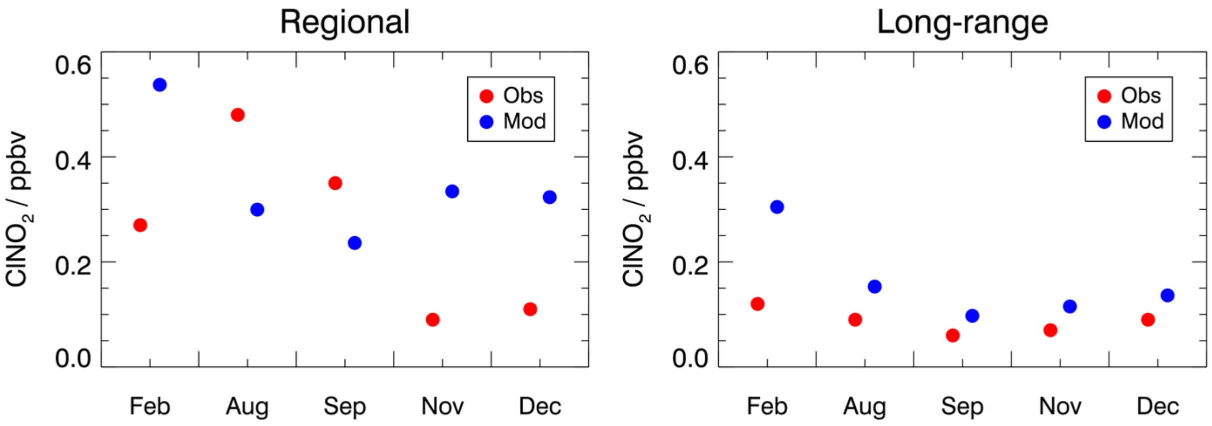

Figure S10. Comparison between observed and modelled $ClNO_2$ for the regional (left) and long-range (right) transportation air masses. Model results are calculated as done in Fig. 6 in main text but measured O_3 concentrations and temperature data are used as input.

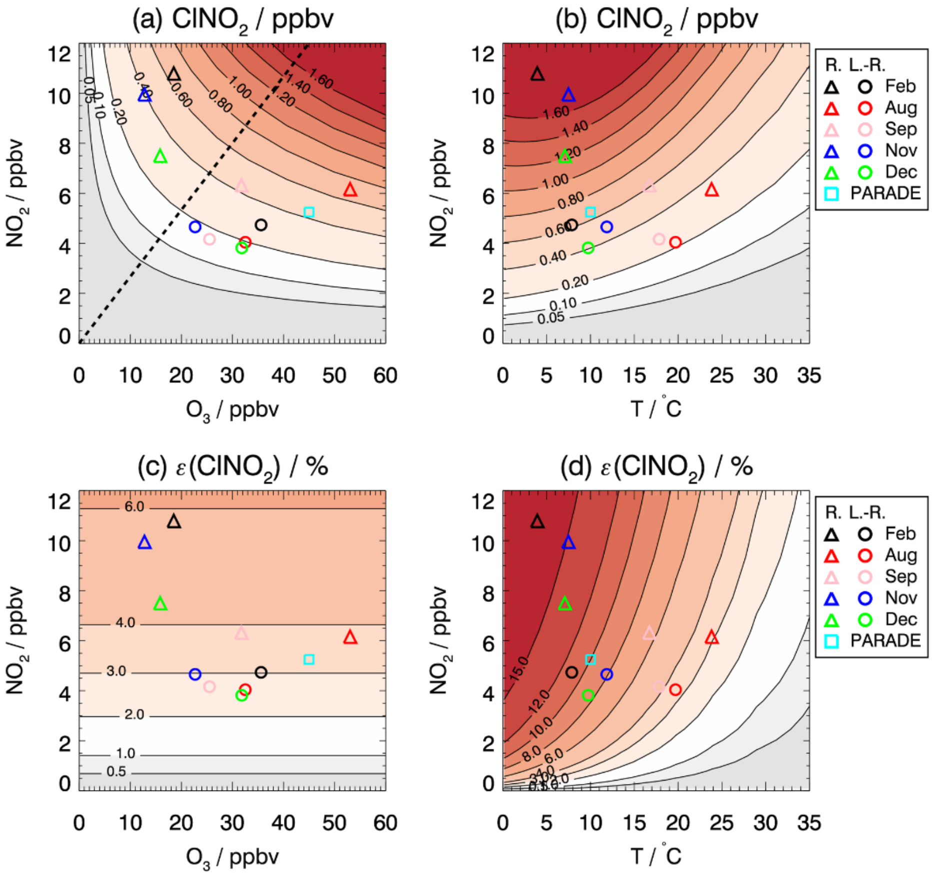

Figure S11. Same as Fig. 6 but the NO_3 radical chemical loss rate constant is decreased from 0.004 s^{-1} to 0.002 s^{-1}.

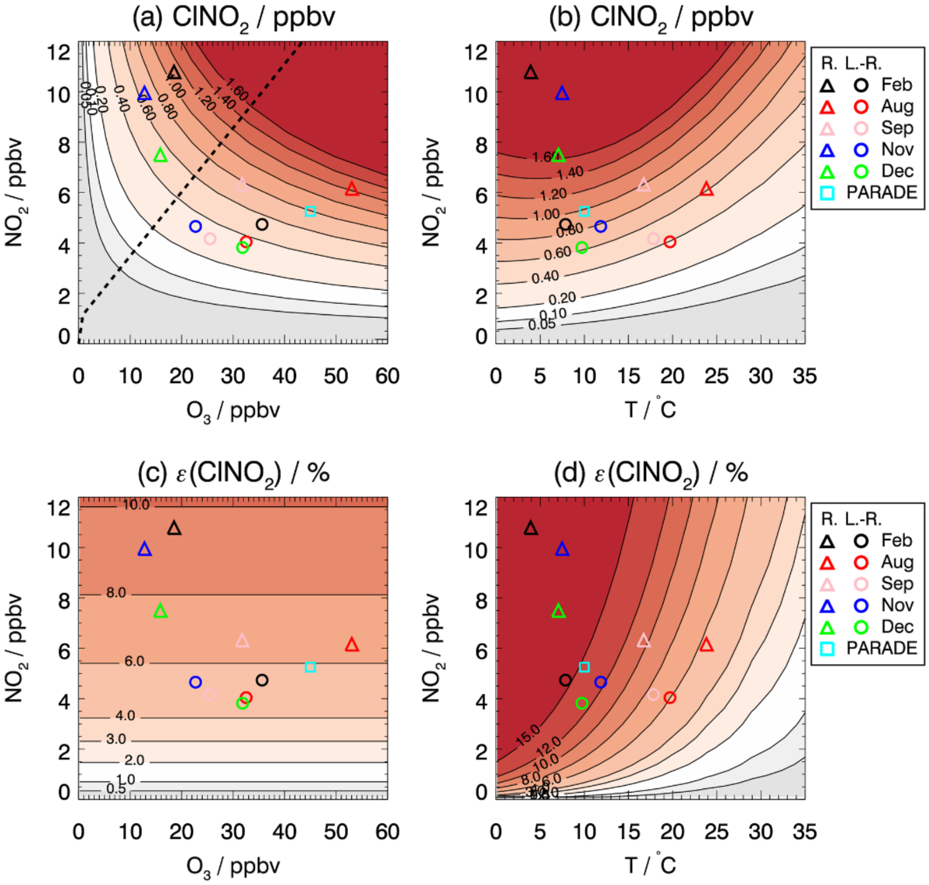

Figure S12. Same as Fig. 6 but the N_2O_5 heterogeneous uptake coefficient on aerosol is increased from 0.01 to 0.04.

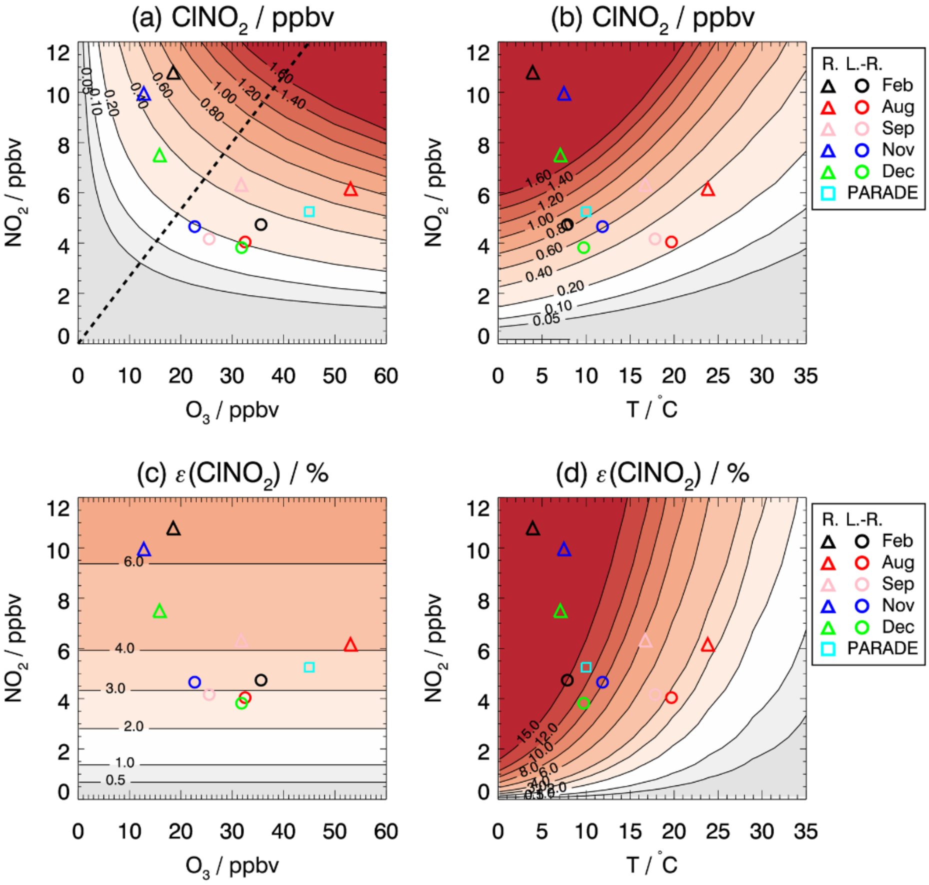

Figure S13. Same as Fig. 6 but the yield of ClNO$_2$ in the heterogeneous reaction of N$_2$O$_5$ on aerosol is increased from 0.5 to 1.0.

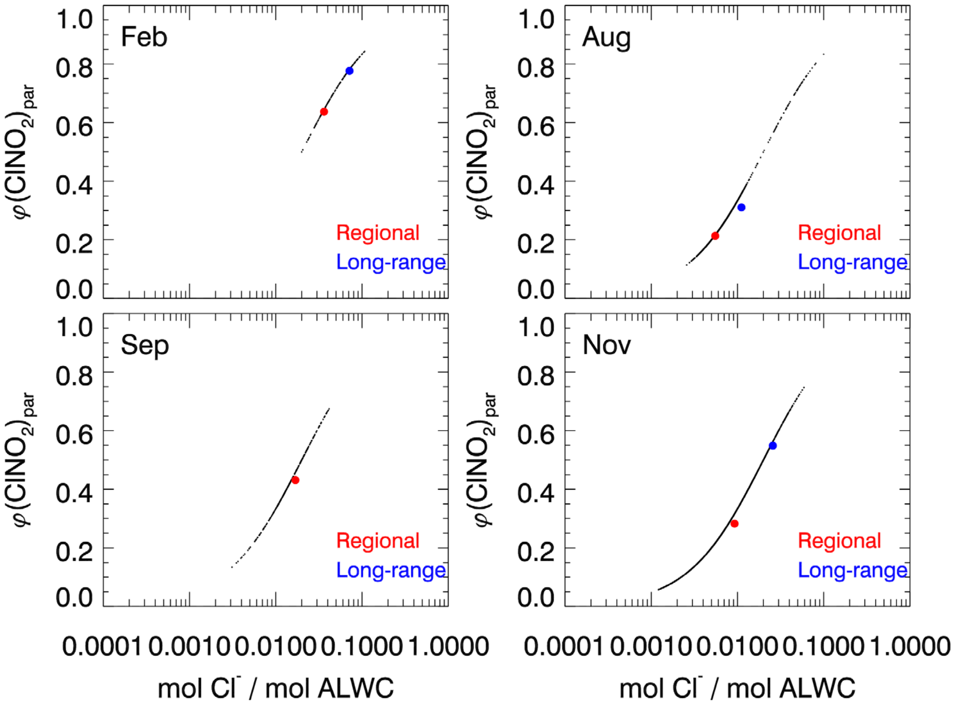

Figure S14. Scatter plot of calculated $ClNO_2$ yield ($\varphi(ClNO_2)$) versus the ratio between Chloride and aerosol liquid water content. Parametrized $\varphi(ClNO_2)$ is calculated following literatures recommendation (Bertram and Thornton, 2009;Mielke et al., 2013;McDuffie et al., 2018). Red and blue dots denote the average for the regional and long-range transported air masses, respectively. In September, the data for Long-range air masses case is missing due to the lack of simultaneous aerosol chemical composition measurement.

References:

Bertram, T. H., and Thornton, J. A.: Toward a general parameterization of N2O5 reactivity on aqueous particles: the competing effects of particle liquid water, nitrate and chloride, Atmos. Chem. Phys., 9, 8351-8363, 10.5194/acp-9-8351-2009, 2009.

Kercher, J., Riedel, T., and Thornton, J.: Chlorine activation by N2O5: simultaneous, in situ detection of ClNO2 and N2O5 by chemical ionization mass spectrometry, Atmos. Meas. Tech., 2, 193-204, 10.5194/amt-2-193-2009, 2009.

McDuffie, E. E., Fibiger, D. L., Dubé, W. P., Lopez Hilfiker, F., Lee, B. H., Jaeglé, L., Guo, H., Weber, R. J., Reeves, J. M., Weinheimer, A. J., Schroder, J. C., Campuzano-Jost, P., Jimenez, J. L., Dibb, J. E., Veres, P., Ebben, C., Sparks, T. L., Wooldridge, P. J., Cohen, R. C., Campos, T., Hall, S. R., Ullmann, K., Roberts, J. M., Thornton, J. A., and Brown, S. S.: ClNO2 Yields From Aircraft Measurements During the 2015 WINTER Campaign and Critical Evaluation of the Current Parameterization, J. Geophys. Res., 123, 12,994-913,015, 10.1029/2018jd029358, 2018.

Mielke, L. H., Stutz, J., Tsai, C., Hurlock, S. C., Roberts, J. M., Veres, P. R., Froyd, K. D., Hayes, P. L., Cubison, M. J., Jimenez, J. L., Washenfelder, R. A., Young, C. J., Gilman, J. B., de Gouw, J. A., Flynn, J. H., Grossberg, N., Lefer, B. L., Liu, J., Weber, R. J., and Osthoff, H. D.: Heterogeneous formation of nitryl chloride and its role as a nocturnal NOx reservoir species during CalNex-LA 2010, J. Geophys. Res., 118, 10,638-610,652, 10.1002/jgrd.50783, 2013.

Slusher, D. L., Huey, L. G., Tanner, D. J., Flocke, F. M., and Roberts, J. M.: A thermal dissociation–chemical ionization mass spectrometry (TD-CIMS) technique for the simultaneous measurement of peroxyacyl nitrates and dinitrogen pentoxide, Journal of Geophysical Research: Atmospheres, 109, 10.1029/2004jd004670, 2004.

Song, S., Gao, M., Xu, W., Shao, J., Shi, G., Wang, S., Wang, Y., Sun, Y., and McElroy, M. B.: Fine-particle pH for Beijing winter haze as inferred from different thermodynamic equilibrium models, Atmos. Chem. Phys., 18, 7423-7438, 10.5194/acp-18-7423-2018, 2018.